International Journal of Material Forming (2024) 17:38
https://doi.org/10.1007/s12289-024-01840-0

ORIGINAL RESEARCH

Numerical simulation and experimental validation of microstructure evolution during the upsetting process of a large size martensitic stainless steel forging

Simin Dourandish[1] · Henri Champliaud[1] · Jean-Benoit Morin[2] · Mohammad Jahazi[1]

Received: 5 September 2023 / Accepted: 21 May 2024 / Published online: 18 June 2024

Abstract
The microstructure evolution, plastic deformation, and damage severity during the open die hot forging of a martensitic stainless steel were investigated using finite element (FE) simulation. A microstructure evolution model was developed and combined with a visco-elastoplastic model to predict the strain, the strain rate, and the temperature distribution, as well as the volume fraction and the size of dynamically recrystallized grains over the entire volume of an industrial size forging. The propensity to damage during hot forging was also evaluated using the Cockcroft & Latham model. The three models were implemented in the FE code and the results analyzed in terms of microstructure inhomogeneity and stress levels in different regions of the forging. A good agreement was obtained between the predicted and the experimental results, demonstrating that the simulation provided a realistic representation of the forging process at the industrial scale.

Keywords Microstructure-based FEM modeling · Martensitic stainless steel · Microstructure evolution · Dynamic recrystallization · Hot forging · Finite element simulation · Damage analysis

Introduction

Critical components, such as turbine shafts made of high strength steels, are produced by ingot casting followed by open die forging [1]. The objective of the latter is to break down the porous and heterogeneous as-cast microstructure in a bid to produce a consolidated microstructure with uniform grain sizes across the entire volume of the forged piece [2]. Static recrystallization (SRX) and dynamic recrystallization (DRX) are the main phenomena resulting in the formation of finer grains. In recent years, the demand for ever larger size ingots has increased significantly, resulting in higher levels of heterogeneity and casting defects. In this context, the selection of the open die forging parameters, namely, strain, strain rate, and temperature, is of paramount importance [3, 4]. Indeed, while it is possible to obtain a uniform grain size distribution in small to medium size bars, when it comes to larger diameters measuring more than 50 cm, [5], a non-uniform grain size distribution is commonplace. Such variations often result in non-conformities, and even part rejection.

During the same period, numerical simulation has proven effective in analyzing the deformation behavior and microstructure development process during hot deformation, thereby reducing the need for large scale experimental trials, [6–10]. Specifically, Jiang et al. [6] used FE simulation to study grain size evolution during hot forming of an Al-1% Mg alloy. They validated their simulation results by using optical microscopy and found an error of around 7%. Cho et al. [7] developed a rigid viscoplastic FE model to predict grain size evolution and recrystallization behaviors during thermomechanical processing of a die steel. They studied the effect of work hardening and holding time on grain growth with experimental validation done using optical micrography technique. Na et al. [8] developed a 3D FEM and predicted grain size evolution during the forging of a superalloy blade and studied the effect of δ phase dissolution temperature on grain boundary movement. Chen et al. [9] simulated the upsetting process of X20Cr13 steel on laboratory scale samples and reported that the DRX volume fraction and grain size were non-uniformly distributed after

✉ Mohammad Jahazi
mohammad.Jahazi@etsmtl.ca

[1] Department of Mechanical Engineering, École de technologie supériere, 1100 Notre-Dame West, Montreal, QC H3C 1K3, Canada

[2] Finkl Steel-Sorel Inc, 100 McCarthy, Saint-Joseph-de-Sorel, QC J3R 3M8, Canada

this forming process, and that the heterogeneity increased with the complexity of the product shape. Lin et al. [10] simulated the hot upsetting process of a 42CrMo steel and concluded that the microstructure evolved unevenly at the end of the process, and that the strain rate and the deformation temperature are the critical factors for the evolution of the microstructure. They also found that the maximum deformation degree occurred at the center of the cylindrical sample, and the material was fully recrystallized at this location. In all the above studies, grain size changes were quantified using optical microscopy and image analysis. In one of the studies, the authors used optical microscopy to technique to determine the experimental grain size.

Some researchers have also reported that a partially recrystallized microstructure influences the strength of the grain and can cause the nucleation of voids, their coalescence, and further evolution into microcracks, which get coarser, and eventually result in fractures [11–13]. To quantitatively predict the ductile fracture condition and the region facing the greatest risk of cracking, different damage criteria, have been proposed [14–18], (https://www.transvalor.com/). Cockcroft and Latham [14] proposed a damage criteria for hot deformation, based on the fracture strain and maximum tensile stress. Oyane et al. [15] proposed a ductile fracture criteria for cold metal working processes that is based on fracture strain of pore-free and porous materials. Brozzo et al. [16] developed and proposed a new method for the prediction of damage and forming limit diagrams during sheet metal forming. Clift et al. [17] used fracture criteria, based on continuum fracture, to predict fracture initiation during metal working processes, such as upsetting and extrusion. Freudenthal [18] developed a criteria to predict the inelastic behavior of solids in plastically deformable structures. Among the above fracture models, Cockcroft-Latham and Brozzo are the most used in hot forging applications. According to the above damage criteria, cracks should be anticipated when the cumulative damage reaches and exceeds the associated critical damage value (https://www.transvalor.com/).

The above literature review demonstrates the strong correlations between the hot forging parameters, microstructure evolution, and susceptibility to cracking; however, no comprehensive research has been conducted to analyze these changes for large size parts, either experimentally or numerically. In particular, no such work has been reported for large size forged ingots of martensitic stainless steels (MSS) that are used for critical components in the energy and transportation industries.

The present study aims to fill this gap and focuses on the application of constitutive models of a martensitic stainless steel recently developed and published by the present authors [19] to the hot forging of a large size industrial scale ingot. Specifically, the effects of thermomechanical parameters on microstructure evolution and grain size during the upsetting step, where the most significant microstructural changes take place, are considered by coupling the physics-based microstructural model with a visco-elastoplastic mechanical model. The models are then implemented into the FEM code, through the development of an original user subroutine (UMAT) forming simulation software application. Variations in temperature, stress, effective strain, damage, DRX fraction, and DRX grain size are thus predicted. Furthermore, the simulation results are validated by comparisons with experimental results.

Materials, methods, and model setup

Compression tests and microstructural characterizations

Finkl Steel (Sorel, Quebec, Canada) provided the materials used in this investigation. The chemical composition of the alloy X12Cr13 is shown in Table 1. AISI410 is also called X12Cr13.

Hot compression tests were conducted on cylindrical samples measuring 10 mm and 15 mm in diameter and height, respectively, using a Gleeble-3800 thermomechanical simulator machine. The samples were prepared from an industrial size forged bar [19]. All thermomechanical processing parameters were selected according to the industrial forging process. Specifically, a temperature range of 1050–1200 °C at intervals of 50 °C and a strain rate of 0.001–1 s^{-1} were used. After the tests, the experimental data were used to develop the constitutive material model needed to predict the flow stress, and at the simulation stage. The accuracy and validity of the predicted material model was ensured through its comparison ed with the experimental results data [19]. The samples were cut parallel to the compression axis by a precision cutter machine for microscopic examination. The specimens were etched with a Vilella solution composed of 1gm $(O_2N)_3C_6H_2OH$, 5 ml HCL, and 100 ml C_2H_5OH, for approximately 25 s. The microscopic images were obtained using an Olympus LEXT OLS4100 laser confocal microscope. The Microstructural Image Processing (MIP4) software (https://en.metsofts.ir/index.html) was used to determine the grain size before and after deformation.

Table 1 Chemical composition of X12Cr13 (wt%)

C	Mn	Cr	Si	*P*	Mo	Cu	Ni
0.14	1.03	11.71	0.25	0.02	0.19	0.15	0.48

Material flow analysis

To accurately predict the material flow behavior of the investigated steel, different constitutive models, such as Hansel-Spittel and Johnson-Cook that are commonly implemented in FE software packages, were investigated [20]. After the predicted flow stress and the stress measured from the experimental tests were compared, an Arrhenius-type model was found to be the most accurate constitutive model. This model is a strain-dependent relationship that relates the strain rate, temperature, and activation energy through the following equation [21]:

$$\sigma = \frac{1}{\alpha} ln\left\{ \left(\frac{Z}{A}\right)^{\frac{1}{n}} + \sqrt{\left(\frac{Z}{A}\right)^{\frac{2}{n}} + 1} \right\} \quad (1)$$

And Z is:

$$Z = \dot{\varepsilon}\ exp\left(\frac{Q}{RT}\right) = A[sinh(\alpha\sigma)]^n \quad (2)$$

where Z is the Zener-Hollomon parameter, Q is the activation energy required to overcome deformation barriers, A, α, and n are material constants, R is the universal gas constant, T is the temperature, $\dot{\varepsilon}$ is the strain rate, and σ is the applied stress.

Numerical analysis of microstructure evolution

Softening processes such as DRX and DRV occur during hot metal working operations such as hot rolling, extrusion, and forging. For materials with low or medium stacking fault energy (SFE) such as stainless steel, DRX is the dominant softening process that takes place when a critical deformation, ε_c, is reached [22]. The DRX fraction during deformation can be calculated by relating the strain, strain rate, deformation temperature, and initial grain size. The equations in this context are based on the JMAK model [23]:

$$X = 1 - e^{-b.t^n}$$

where b and n correspond to the Avrami coefficients. This equation was coded with a FORTRAN 90 user subroutine (https://www.fortran.com) into the Forge NxT 3.1® software. The constants of the equations, reported in Table 2, were calculated using flow stress data from the hot compression tests, detailed in a recent publication by the present authors [19].

The parameters listed in Table 2 were determined through the following procedure: first, the hardening rate was calculated from the flow stress curves obtained at different temperatures and strain rates. Next, the relationship between hardening rate and strain was plotted to identify the critical strain for dynamic recrystallization, determined as the inflection point on the curves. Constitutive equations for the critical strain (ε_c), DRX fraction (X_{drx}), and DRX grain size (D_{drx}) were then formulated as functions of initial grain size (d_0) and the Zener-Holloman parameter (Z). Coefficients and exponents for these equations were determined using regression analysis. The final equations for DRX are presented in Table 2. Figure 1 shows the procedure used in the numerical analysis for microstructural evolution prediction.

The material parameters used in the numerical analysis and implementation in the FEM model were: Initial grain size, d_0 (μm), DRX grain size, D_{drx} (μm), Temperature, T (°C), Critical strain, ε_c, Strain rate, $\dot{\varepsilon}$ (1/s), and DRX fraction (X_{drx}). The details of the experimental methodology used to determine the above parameters can be found in a recent publication by the present authors [19]. The Parameters listed in Table 2 were combined with the microstructural equations and implemented into the software. The selection of the thermomechanical processing parameters is representative of the actual industrial forging process. The ingot temperature was measured by a high-performance thermal camera. The reading temperature started when the ingot was taken out of the forging furnace and proceed until the end of the forging operation, for a total of 3 min. For the selection of the strain and strain rate, the hydraulic press data, press pressure and press position that were

Table 2 Equations describing the microstructure evolution [24]

Parameters	Equation
Critical strain	$\varepsilon_c = 0.626 \times d_0^{0.576} \dot{\varepsilon}^{-0.058} exp\left(\frac{50{,}344}{R.T}\right)$
Zener-Hollomon	$z = \dot{\varepsilon}\ exp\left(\frac{430{,}258}{RT}\right)$
Dynamic recrystallization fraction	$X_{drx} = 1 - exp\left(-0.693\left(\frac{\varepsilon - \varepsilon_c}{\varepsilon_{0.5}}\right)^2\right)$
50% recrystallization	$\varepsilon_{0.5} = 5.05 \times 10^{-3} d_0^{0.47} \dot{\varepsilon}^{0.12} exp\left(\frac{26{,}128}{R.T}\right)$
Recrystallized grain size	$D_{drx} = 30,500 \dot{\varepsilon}^{0.242} exp\left(\frac{-78{,}572}{RT}\right). X_{drx}^{0.191}$

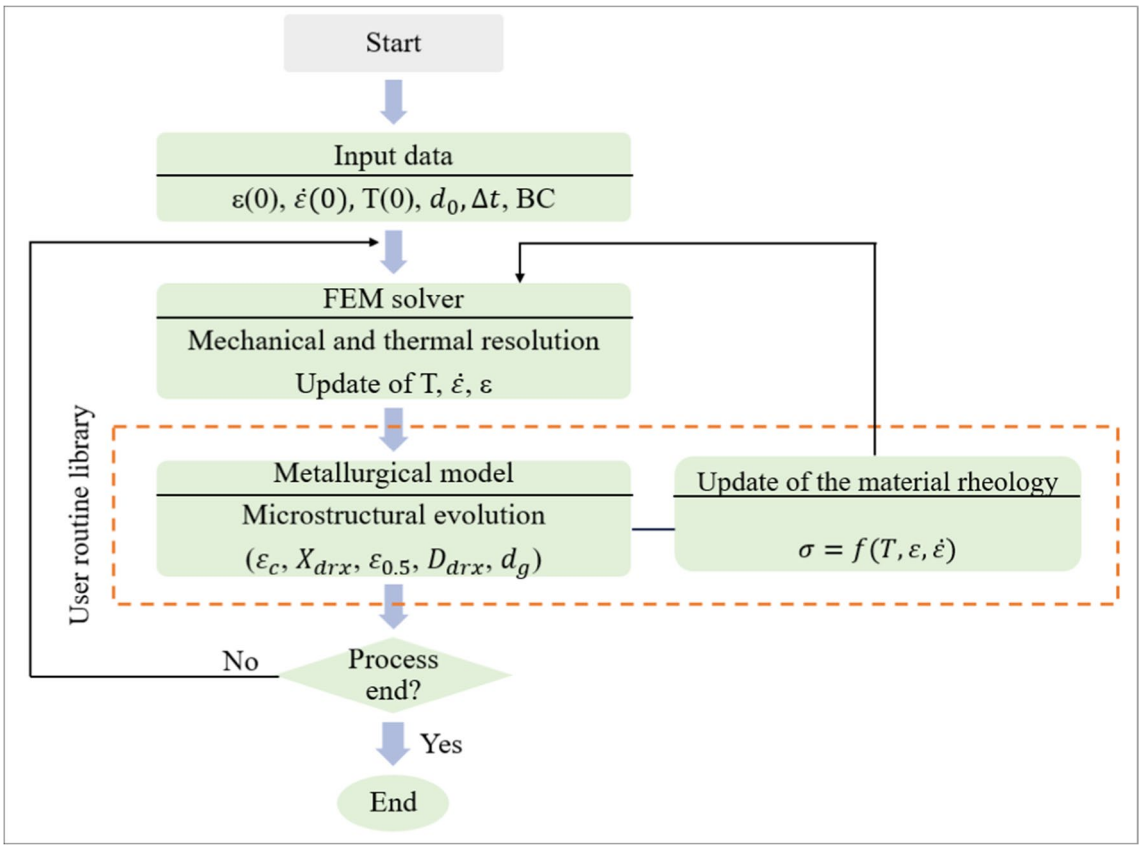

Fig. 1 Numerical analysis procedure to predict the microstructural evolution using Forge NxT 3.1® software

continuously recorded during the forging operation were analyzed, and the applied strain and strain rate in each time segment was determined and used for the design of the laboratory scale experiments.

Boundary conditions for Simulation

The amount of deformation and die velocity were recorded using the Finkl Steel equipment during the open die forging, as shown in Fig. 2a. The open die forging process (upsetting) was done using a 5000-ton press capacity, and Fig. 2b shows the forging process setup. The temperature was measured by a high-performance thermal imager, ThermoView® pi20, Fig. 2c [25]. Figure 3a shows the as-cast ingot after solidification, which is ready to be transferred to the forging furnace and heated up to forging temperature and held for several hours, for temperature homogenization.

The complete meshed CAD model is shown in Fig. 3b. Due to the presence of symmetric conditions, as shown in Fig. 3b, a quarter of the 13.5 metric ton ingot was modeled and used for the simulation step (Fig. 3c). Six sensors were installed as shown in Fig. 3c to track the results. The 3D linear tetrahedral mesh was selected with volumetric elements, with a fine mesh size to provide high convergence. Table 3 shows the boundary conditions used for the upsetting simulation.

It must be noted that under industrial forging conditions, the ingot is heated up to 1230 °C and the forging starts at 1200 °C. Due to the very large size of the ingot, the temeprature remains almost constant duirng a large part of the upsetting process. As a result, only the results for the 1200 °C are shown here. However, all changes in temperature, strain and strain rate are calculated at any moment duirng the forging process, based on the boundary and initial conditions, throughout the forging process.

Damage analysis

To identify areas susceptible to deterioration during the forging process, the stress and strain states for deformed ingots were determined with the application of a finite element simulation. Among the different existing damage criteria, the Latham-Cockroft damage criterion [14], which has successfully been applied to forging processes, was selected in this study. It involves the standardization

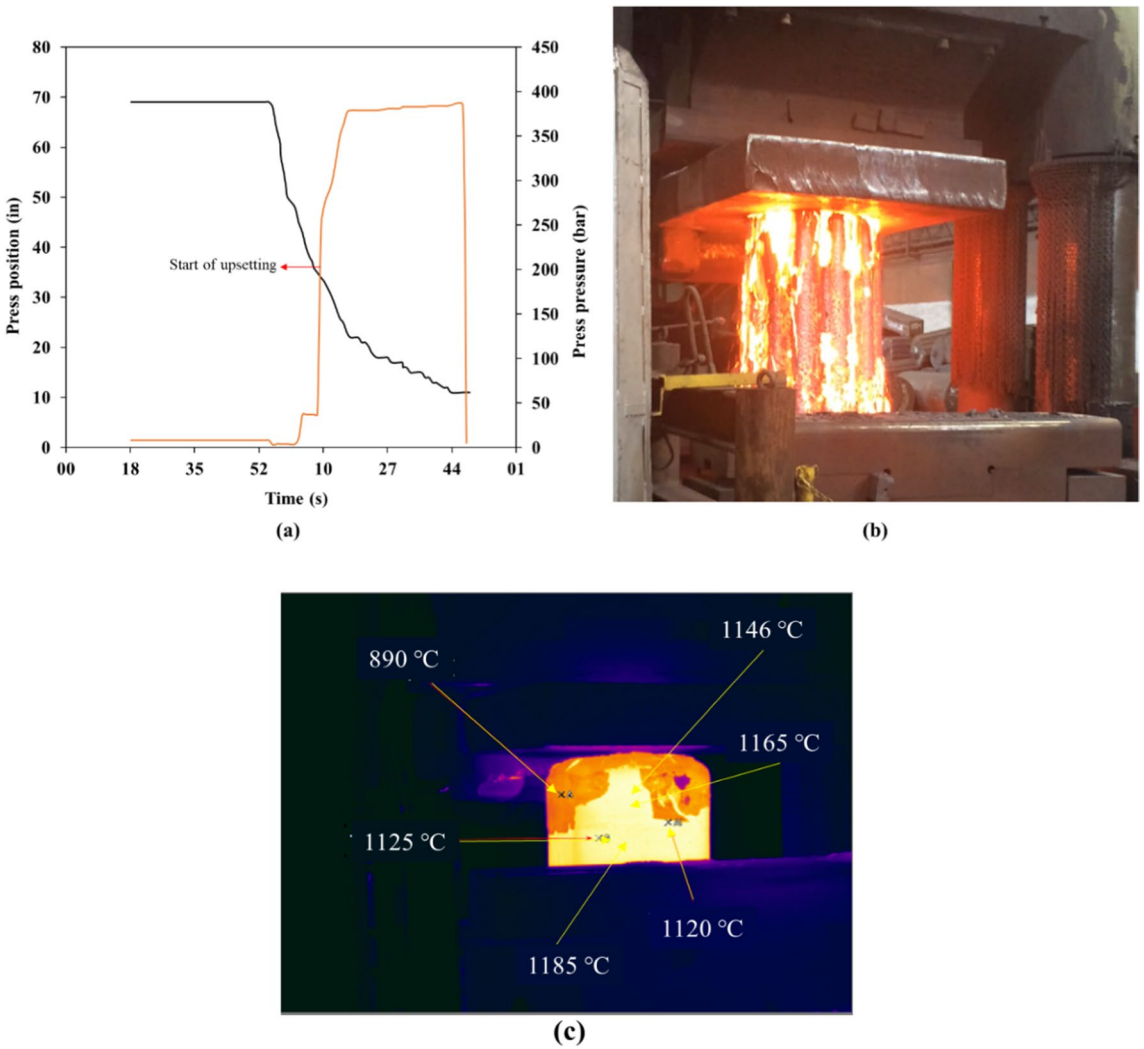

Fig. 2 **a** 5000-ton press data for measuring the simulation parameters; **b** Upsetting process setup (5000-ton press); **c** Image taken by the thermal camera

of stress by dividing the maximum stress by the equivalent stress as follows:

$$C = \int_0^{\bar{\varepsilon}} \frac{\sigma_{max}}{\bar{\sigma}} d\bar{\varepsilon} \tag{3}$$

where $\bar{\varepsilon}$ is the equivalent plastic strain, σ_{max} is the maximum principal stress, $\bar{\sigma}$ is the effective stress. The damage parameter C is a function of temperature, strain rate, and microstructure. Equation (3) was implemented into the software through a user subroutine and utilizes the remeshing function. A higher 'C' value, called the *damage value* hereafter, indicates a higher susceptibility to cracking. The damage value for martensitic stainless steel during hot forging which leads to surface cracking was reported as 0.5 and 0.6 [26].

Results and discussion

To analyze the industrial upsetting process of X12Cr13 stainless steel, simulation data was collected over the duration of the process (0 to 35 s). Six sensors (S 1 to S 6) were positioned along the center axis of the ingot and parallel to the deformation axis. Sensors 1 and 6 were placed near the bottom die and at the point of maximum strain, respectively, while sensors S 2 to S 5 were positioned between sensors S 1 and S 6. Equivalent strain, strain rate, critical strain, DRX fraction, DRX grain size, and average grain size distribution were plotted against time to demonstrate the variation of critical parameters with time and different sensor positions. This analysis is presented in the following subsections.

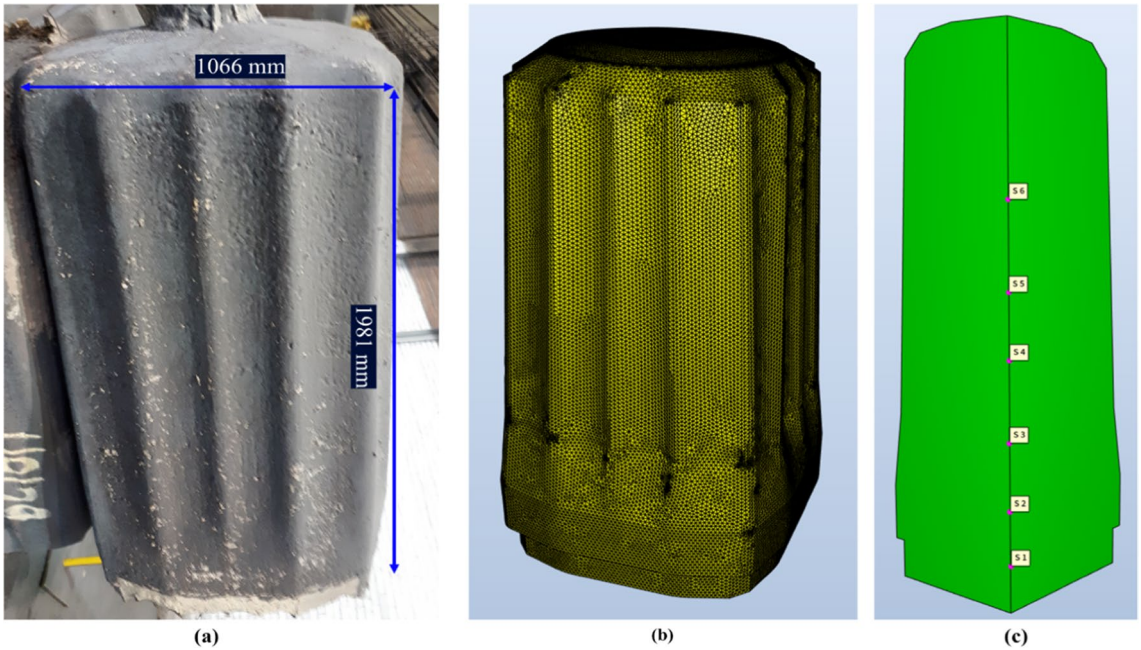

Fig. 3 **a** 1066 mm diameter as-cast ingot; **b** meshed finite element model; **c** ¼ of the model

Table 3 Input data for FEM analysis

Parameters	Value
Temperature (°C)	1200
Friction factor	0.35
Die temperature (°C)	400
Environment temperature (°C)	35
Press velocity (mm/s)	23.35
Initial billet height (mm)	1960
Final billet height (mm)	1143

Strain/Strain rate distribution simulation results during upsetting

Strain distribution contours are shown in Fig. 4a. It can be seen that the contact zones with anvils (upper and lower dies) have lower strain values while the center and upper half of the ingot correspond to highly strained regions. The strain decreases gradually as we approach the surface of the ingot. The sensors are assigned to track parameter changes during the deformation, from the beginning to the end of the process. Figure 4b shows the strain versus time of 6 sensors, with the maximum strain level seen for point S 6. Figure 5a and b show the strain rate contour and the strain rate value of 6 sensors during the upsetting. The average strain rate with the industrial condition is 0.015 s^{-1} for the upsetting process.

Critical strain for the initiation of dynamic recrystallization

Dynamic recrystallization phenomena require that a critical amount of deformation occur at a given temperature. The critical strain equation, ε_c, is shown in Table 2 as a power law. After constant calculations, the equation was implemented into the Forge NxT 3.1® software through a user subroutine. Figure 6a and b represent the map of ε_c and the values of ε_c for the six points. All points, except for S 1, reach the critical value at different process time periods due to the uneven distribution of the strain. The point with the maximum strain, S 6, reaches the critical value sooner than the other points. However, no value appears in the diagram for point S 1 because it is situated in the dead zone, which has not experienced enough deformation for DRX initiation. This means that in this area, DRV is the dominant softening mechanism.

Dynamic recrystallization distribution

Figure 7a shows the map of the DRX volume fraction distribution under industrial deformation conditions. It is revealed that the dynamic recrystallization fraction has a direct relationship with the strain: it rises with increasing strain and falls with decreasing strain. Moreover, the DRX volume fraction distribution is inhomogeneous, due to the inhomogeneous strain distribution, as reported in Fig. 5a. This means that the strain distribution directly affects the microstructural evolution during upsetting. The maximum

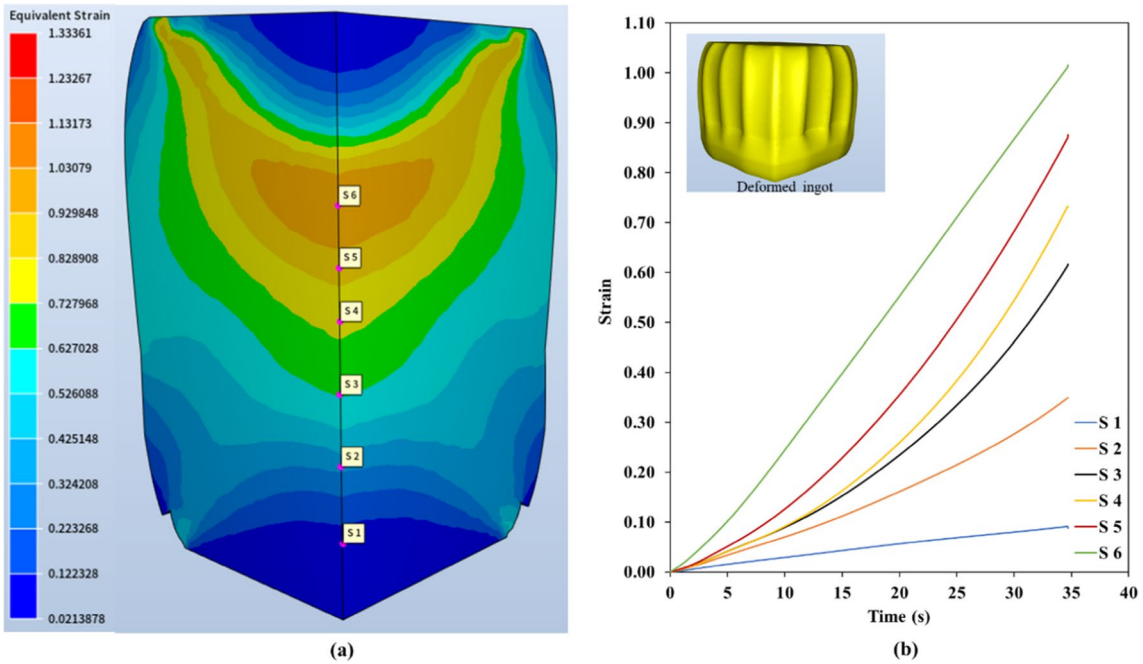

Fig. 4 X12Cr13 stainless steel open die forging simulation results: **a** distribution of equivalent strain; **b** plot of strain evolution of 6 sensors during upsetting

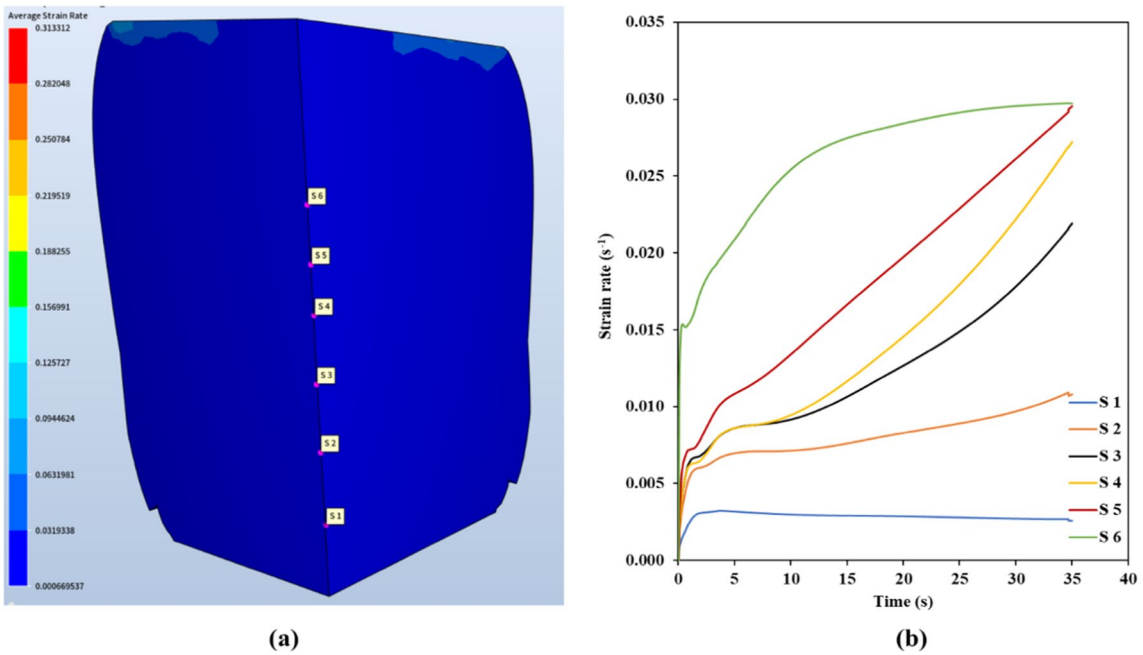

Fig. 5 X12Cr13 stainless steel open die forging simulation results: **a** distribution of average strain rate; **b** plot of strain rate evolution of 6 sensors during upsetting

DRX fraction is located at the center, toward the top of the ingot, where the workpiece experiences its maximum degree of deformation, while the minimum is related to the top and bottom of the ingot in contact with the upper and lower dies.

Figure 7b depicts the DRX fraction of six sensors versus time, and it is seen that the DRX fraction of point S 1 is close to zero, while that of S 6 reaches 100% DRX. The DRX starts at a different time for each point because of the

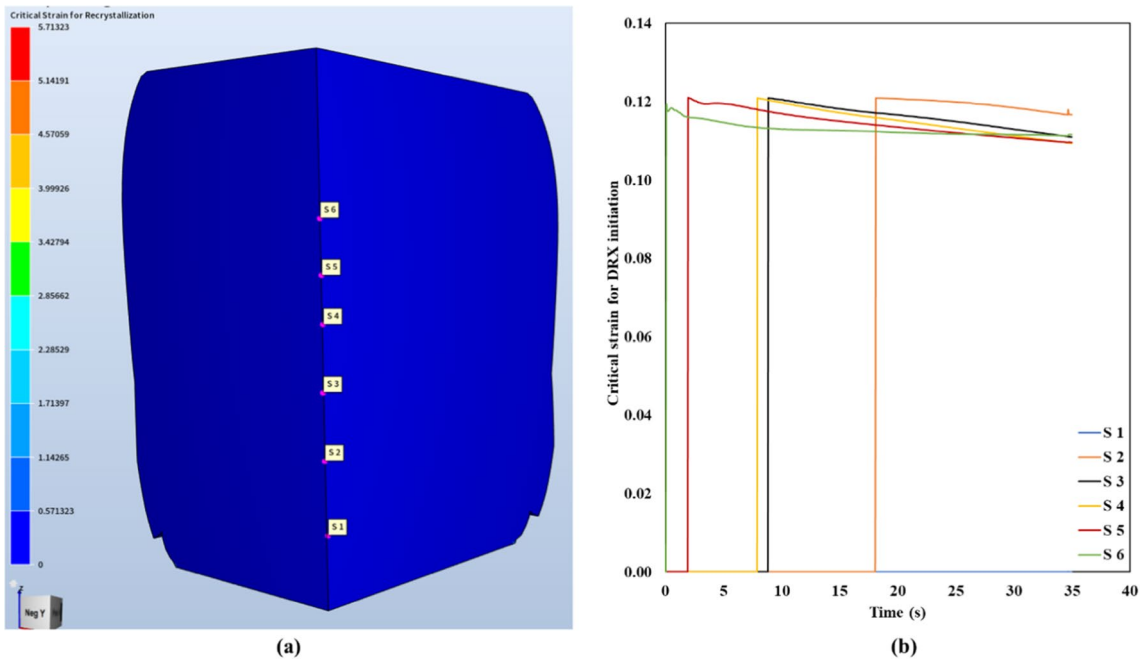

Fig. 6 X12Cr13 stainless steel open die forging simulations results: **a** distribution of critical strain for DRX initiation; **b** plot of critical strain evolution of 6 sensors during upsetting

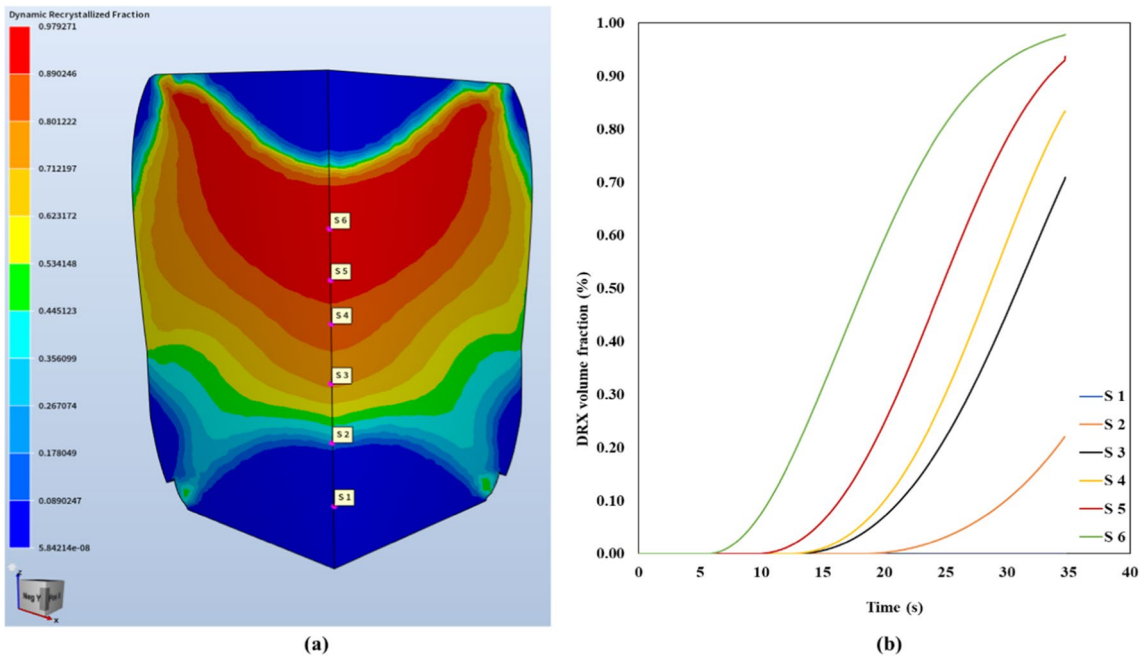

Fig. 7 X12Cr13 stainless steel open die forging simulation results: **a** distribution of DRX at the end of upsetting; **b** plot of DRX fraction evolution of 6 sensors during upsetting

uneven strain distribution, with this start time being sooner for higher strain values than for the other points.

Figure 8 presents a whole model in order to illustrate the different percentages of DRX volume fraction at the end of upsetting, where the material volume does not undergo the DRX phenomenon, and how much of the material is fully recrystallized. The ISO volume corresponds to the amount of recrystallized volume that the software provide these results.

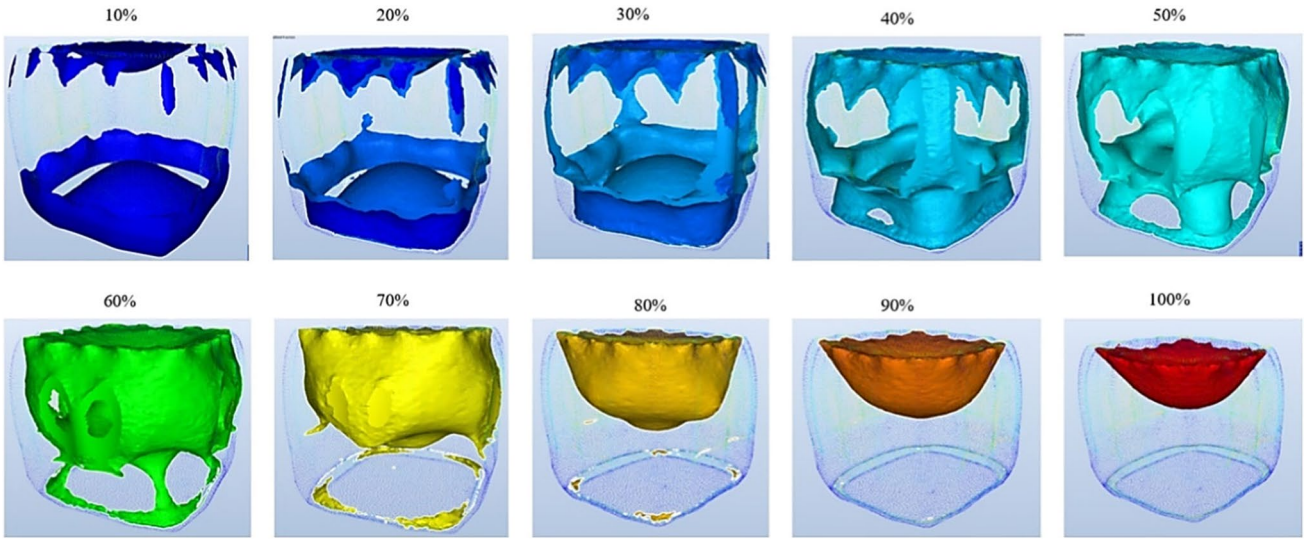

Fig. 8 Iso volume of DRX fraction in different percentages at the end of upsetting

DRX grain size distribution

Figure 9a presents the DRX grain size map. Like previous parameter contours, the grain size distribution is also uneven, and the higher the strain, the bigger the grain size. As the point reaches the critical strain, ε_c, the DRX initiates. Figure 9b shows the moment when DRX grain nucleation occurs; as the deformation proceeds, the nuclei get coarser. In the regions where the nucleation starts sooner, the nuclei have more time to grow, but the points with lower DRX volume fractions have finer grain sizes as the grains are at the start of the recrystallization stage. In general, the nuclei start off very fine and continue growing until the next recrystallization cycle. The DRX grain size, therefore, increases as the DRX percentage increases. For

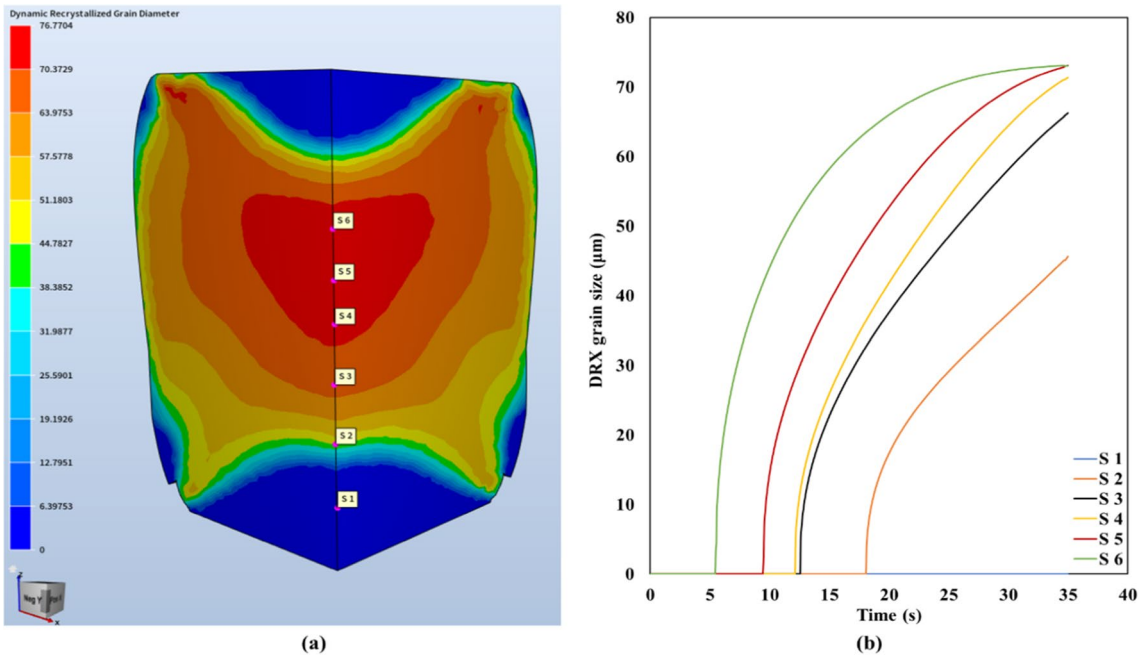

Fig. 9 X12Cr13 stainless steel open die forging simulation results: **a** distribution of DRX grain diameter at the end of upsetting; **b** plot of DRX grain diameter evolution of 6 sensors during upsetting

the zones with complete DRX, the grain size is around 73 µm, which is 70.8% smaller than the initial grain size.

Distribution of average grain diameter

This section shows the grain size distribution of recrystallized and non-recrystallized (dead zone) materials. Figure 10a shows the grain size map, with the red zones experiencing minimum deformation. As shown in Fig. 10b, the grain size at S 1, which is in the red zone, remained unchanged from its initial value.

The damage analysis was carried out to find the area's most sensitive to crack formation. In the damage criteria, it was assumed that a crack is initiated in a deformed material only

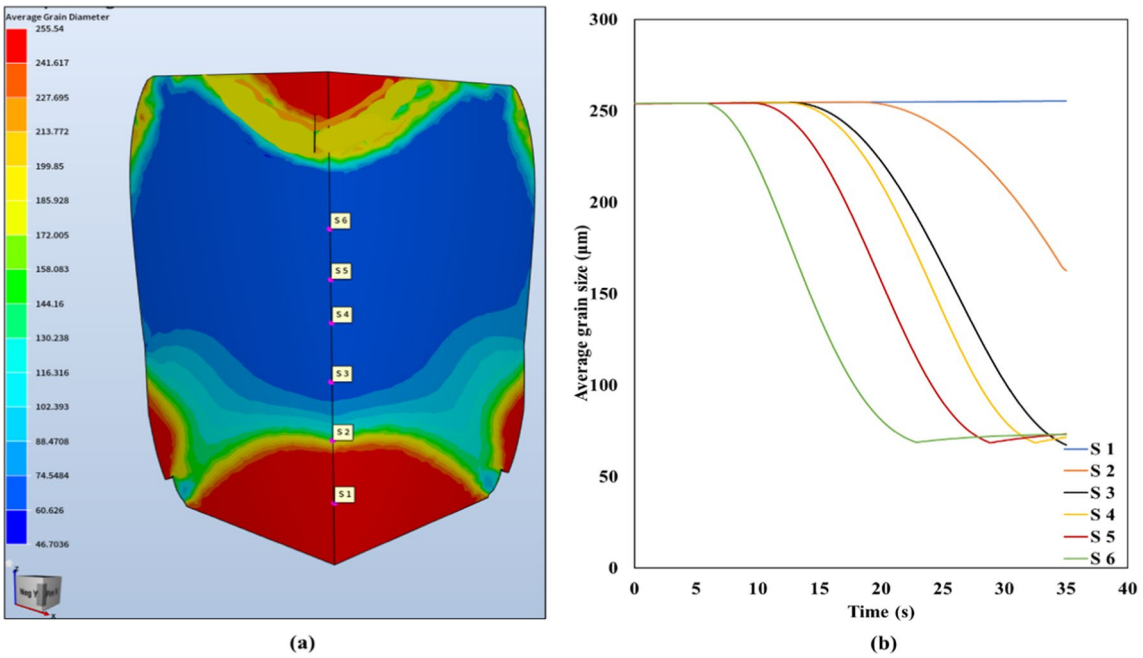

Fig. 10 X12Cr13 stainless steel open die forging simulation results: **a** distribution of average grain diameter at the end of upsetting; **b** plot of DRX fraction evolution of 6 sensors during upsetting

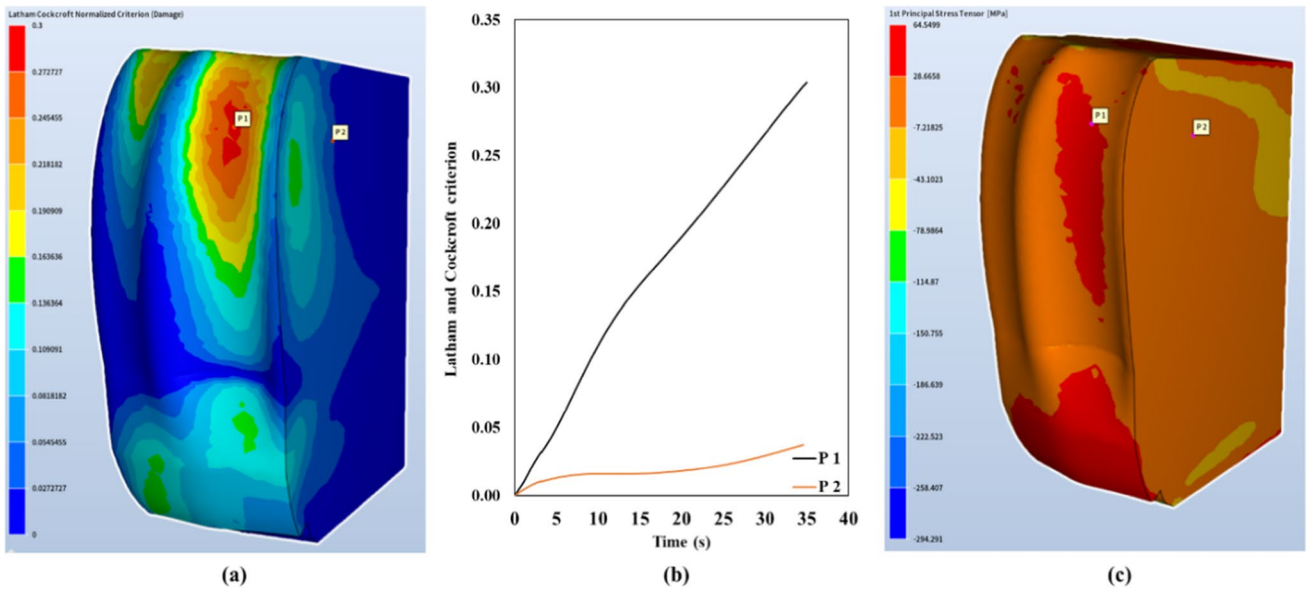

Fig. 11 X12Cr13 stainless steel open die forging simulation results: **a** distribution of Cockcroft and Latham damage criteria; **b** plot of damage factors evolution of two sensors on the surface and inside of the ingot; **c** distribution of maximum principal stress

when a threshold value, defined based on the criteria used, is exceeded [1, 27]. Figure 11a shows the contour of the damage factor for the Latham Cockcroft damage criteria at the end of upsetting. As expected, the surface of the ingot is most likely to undergo crack formation, which means that the surface of the ingot is in danger of cracking. Figure 11b depicts two sensors selected on the surface and inside the ingot, with two different cracking risk levels. In Fig. 11c, the area with the highest cracking risk, the surface, experiences a higher maximum principal stress. This means that the maximum level of tensile stress was achieved on the surface of the ingot. The combination of a non-uniform microstructure evolution and high tensile stresses could lead to the formation of surface cracks. Therefore, based on the above analysis, it is possible to develop new forging schedules that would result in more uniform microstructures and higher mechanical properties while avoiding surface cracks during the deformation process.

Verification of the simulation results with experimental measurement

Compression tests were conducted using the Gleeble-3800 thermomechanical simulator machine. In a previous study [19], the Arrhenius model was validated as a predictive constitutive equation by comparison with experimental results, and the model was implemented into the simulation software, with good agreement. The DRX fraction and critical strain for the initiation of DRX were calculated for all deformation conditions. The characteristic points, including the peak stress and peak strain, critical stress and strain, and the maximum softening rate, were calculated using the methodology proposed by Poliak and Jonas, named the *double-differentiation technique* [25]. The microstructure evolution of the deformed sample was characterized for comparison with the microstructure-based FEM model prediction results. Figure 12a and b show the microstructure before deformation and the cross-section of the deformed samples in the 1200 °C–0.1 s^{-1} condition, respectively. Three zones were selected to show non-recrystallized, partially recrystallized, and fully recrystallized materials under

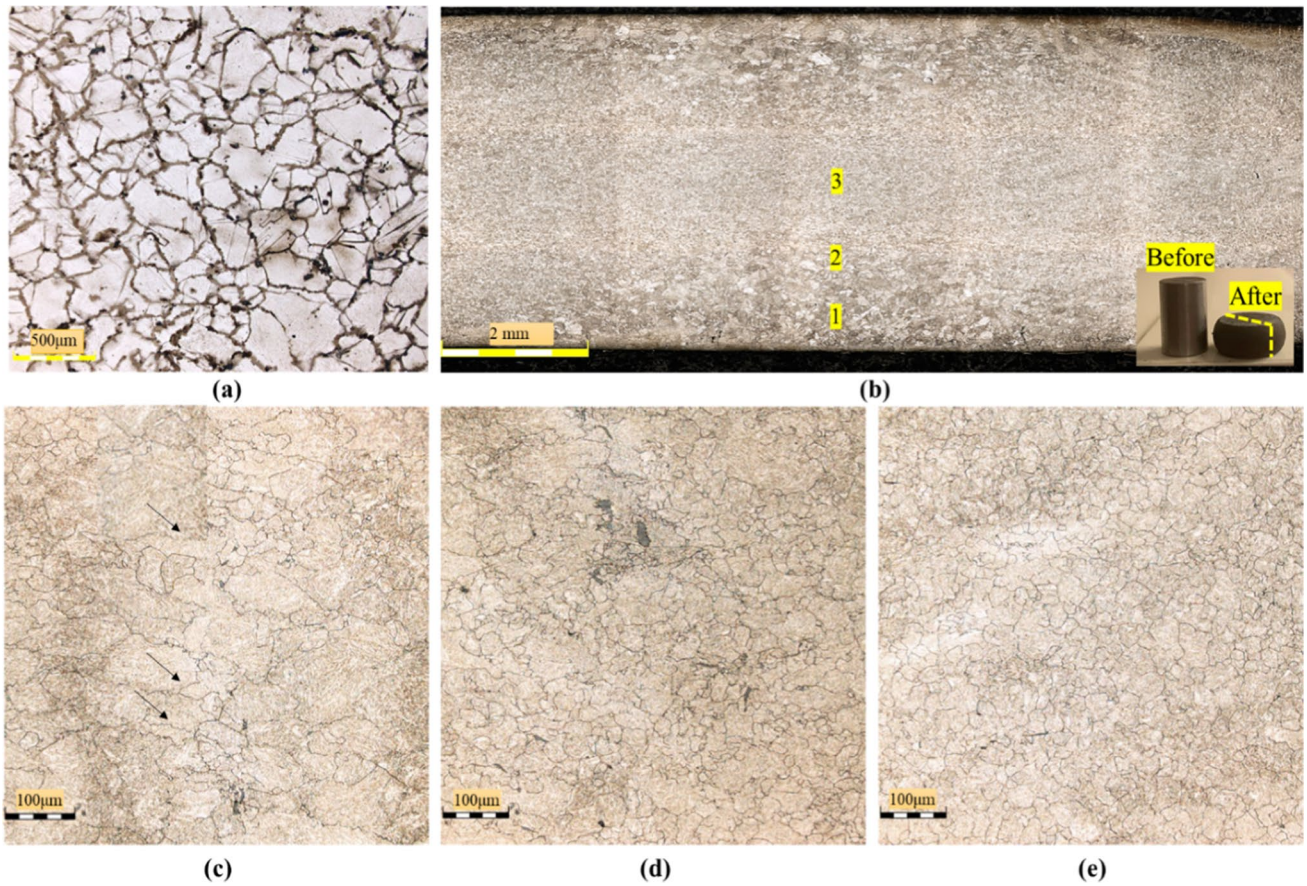

Fig. 12 **a** Initial microstructure before hot compression test; **b** stitching image of a cross-section of the deformed sample; **c** unchanged microstructure of zone 1 with serrated grain boundary; **d** mixed microstructure of zone 2; **e** fine and uniform microstructure of zone 3

Table 4 DRX grain size at different temperatures and different strain rates at the end of upsetting

Temperature (°C)	Strain rate (s^{-1})	Grain size (μm)
1050	0.001	23.65
	0.01	23.06
	0.1	21.78
	1	20.14
1100	0.001	68.59
	0.01	56.6
	0.1	48.25
	1	25.27
1150	0.001	77.75
	0.01	64.66
	0.1	52.28
	1	40.76
1200	0.001	92.5
	0.01	72.58
	0.1	66.4
	1	39.83

hot compression tests. The microstructure of the dead zones, the top and the bottom in contact with the anvils remained unchanged. However, the serrated grain boundaries (black arrows) in Fig. 12c, zone 1, indicate that the dislocation accumulation and migration have started at these locations, but the degree of deformation is not sufficient to enable the accumulation and nucleation of a nucleus. Figure 12d, zone 2, shows the partial recrystallization, meaning that the DRX starts locally. In this zone, the material reaches the critical strain for DRX initiation, but does not exceed the complete recrystallization strain. Figure 12e, zone 3, shows the center of the deformed sample, which has uniform and fine recrystallized grains, and the material is fully recrystallized in this zone. As can be seen, the recrystallized grains are much finer than the initial grains.

Table 4 shows the grain size of the deformed samples measured by the MIP4 software for all deformation conditions. The grain size increases as the temperature increases and when the strain rate decreases. Figure 13 shows the microstructure of the deformed sample measured by the MIP4 software. The critical strain was measured for the experimental tests, as shown in Table 5.

By comparing the microstructure evolution of the simulation results and the experimental one under similar conditions, it can be seen that the implemented equations for the

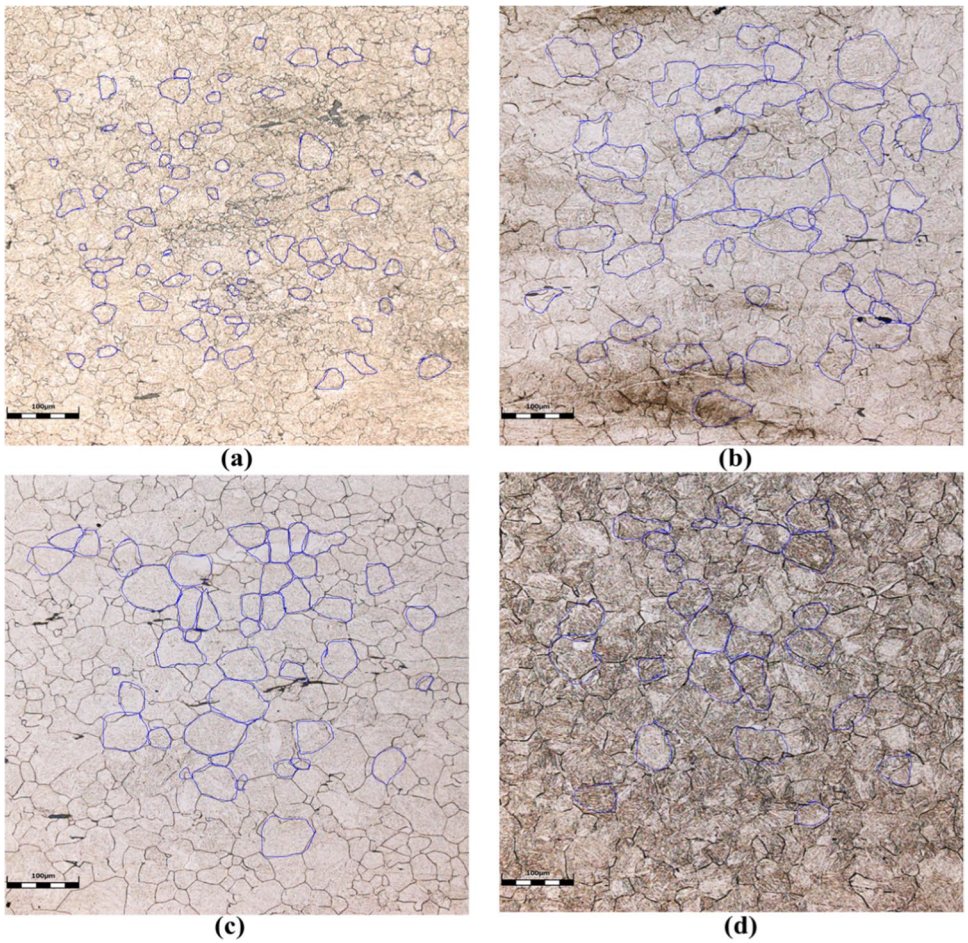

Fig. 13 Microstructure of deformed sample measured by MIP4 at (**a**) 1050 °C–0.1 s^{-1} (**b**) 1100 °C–0.1 s^{-1} (**c**) 1150 °C–1 s^{-1} (**d**) 1200 °C–1 s^{-1}

Table 5 Critical strain for DRX initiation at forging temperature

Temperature (°C)	Strain rate (s^{-1})	ε_c
1200	0.001	0.02
	0.01	0.113
	0.1	0.127

DRX fraction, DRX grain size, and critical strain for DRX initiation could accurately predict the microstructure evolution of a large size ingot.

Figure 14a and b depict the distribution of the damage value over the external surface of a deformed sample and in its central section, respectively. Similar to the simulation results shown in Fig. 11, the damage value is maximum at the surface of the sample. Figure 14c presents the microstructure of the deformed sample at the location with the maximum damage value. As can be seen, the microstructure is composed of a mix of large size and small size grains characteristic of a partially recrystallized microstructure. These microstructure non-uniformities and high damage value of the surface could make this area particularly susceptible to crack formation.

The higher damage value and the presence of an inhomogeneous grain distribution observed at the free deformation surface of the ingot during hot deformation, indicate that cracks were more prone to initiate at the surface. Specifically, the higher damage values around the free deformation surface signifies the presence of higher tensile stresses, as shown in Fig. 11b, while the inhomogeneous grain distribution reveals a combination of recrystallized and non-recrystallized grains near the free deformation surface. At the end of deformation, around the free deformation surface, lower strain is present compared to the center of the specimen. Therefore, partial dynamic recrystallization occurs at the surface, leading to inhomogeneous grain sizes. Due to the combination of the inhomogeneous microstructure and higher damage (tensile stresses) at the surface, which weakens the strength of grain boundaries and the grain interior, surface cracking occurs during the hot deformation of X12Cr13 stainless steel. Similar observations have been reported during high temperature deformation of AISI 410 and AISI 321 stainless steels [13, 26]. Finally, it must be noted that fundamental mechanisms governing the kinetics of DRX and related softening processes that take place during hot deformation were not studied in the framework of the present research and require a separate study similar to the one reported in a recent publication [28].

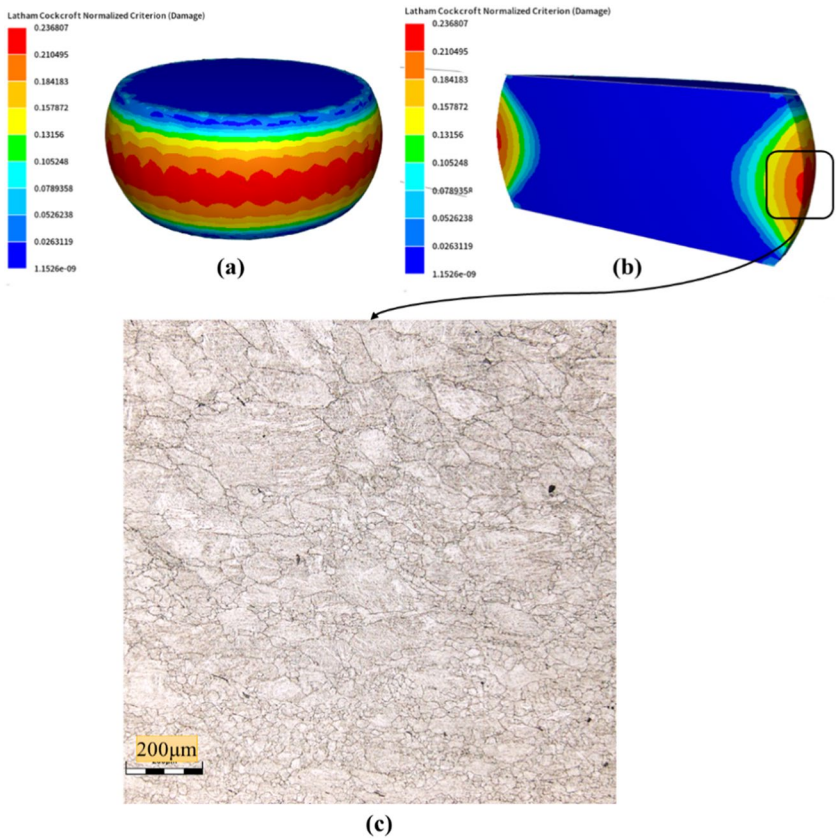

Fig. 14 Distribution of X12Cr13 stainless steel Cockcroft and Latham damage criteria; **a** whole sample; **b** inside deformed sample; **c** micrographs of the deformed sample with a maximum damage value

Conclusions

In this study, numerical simulation and experimental studies were carried out on the upsetting process at a high temperature of X12Cr13 stainless steel. The evolution of the working parameters involved was analyzed, leading to the following conclusions:

1. The constitutive equation and microstructure evolution models were implemented into the finite element code through a user subroutine and a coupling of models showed very good agreement with the experimental findings for the investigated steel.
2. The simulation results allowed to develop a detailed map of the temperature, strain, and strain rate over the entire volume of the large size ingots and specifically showed that more than 80% of the ingot was recrystallized at the end of upsetting. Specifically, the simulation results, validated by experimental observations of the microstructure, showed that in the regions with mixed large and small grain sizes, such as the surface region, the material is more sensitive to cracking, as evidenced by higher damage values.
3. The damage analysis results showed that cracking susceptibility is higher in the regions with mixed microstructures (recrystallized and non-recrystallized). Such regions are often close to the surface of the forging.

Acknowledgements This research was conducted in close collaboration with Finkl Steel-Sorel as the industrial partner. The authors would like to thank Finkl Steel-Sorel for providing the samples and for the extensive support by the research and development and technical departments. Part of the financial support for the work was received from Mitacs through a grant (IT164670), for which we express our sincere gratitude. We also thank Mr. Nicolas Poulain from Transvalor Inc. for his help in implementing a new model in the Forge NxT 3.1® software.

Author contributions **Simin Dourandish**: Conduct of experimental tests and numerical analysis, methodology, writing, review and editing of paper. **Henri Champliaud**: Finite element modeling, review, and editing. **Jean-Benoit Morin**: Material provision, technical support, industrial application, review and editing. **Mohammad Jahazi**: Project idea, project definition, review of the methodology and experimental part, supervision, review and editing.

Data availability The datasets used in the present study is available from the corresponding author upon reasonable request.

Declarations

Competing interest The authors declare that they have no known competing financial interests or personal relationships that could have appeared to influence the work reported in this paper.

References

1. Dowson P, Bauer D, Laney S (2008) Selection of materials and material related processes for centrifugal compressors and steam turbines in the oil and petrochemical industry. Proceedings of the 37th Turbomachinery Symposium, Texas A&M University. Turbomachinery Laboratories, pp 189-209
2. Chadha K, Shahriari D, Tremblay R et al (2017) Deformation and recrystallization behavior of the cast structure in large size, high strength steel ingots: experimentation and modeling. Metall Mater Trans A 48:4297–4313. https://doi.org/10.1007/s11661-017-4177-8
3. Jang YS, Ko DC, Kim BM (2000) Application of the finite element method to predict microstructure evolution in the hot forging of steel. J Mater Process Technol 101:85–94. https://doi.org/10.1016/S0924-0136(99)00460-4
4. Ma Q, Lin ZQ, Yu ZQ (2009) Prediction of deformation behavior and microstructure evolution in heavy forging by FEM. Int J Adv Manuf Technol 40:253–260. https://doi.org/10.1007/s00170-007-1337-9
5. Bontcheva N, Petzov G (2003) Microstructure evolution during metal forming processes. Comput Mater Sci 28:563–573. https://doi.org/10.1016/j.commatsci.2003.08.014
6. Jiang WG, Wang GC, Lu SQ, Li JW (2007) Prediction of microstructure evolution of Al-1% mg alloy during hot forming and sequential heat treatment. J Mater Process Technol 182:274–280. https://doi.org/10.1016/j.jmatprotec.2006.08.005
7. Cho JR, Jeong HS, Cha DJ et al (2005) Prediction of microstructural evolution and recrystallization behaviors of a hot working die steel by FEM. J Mater Process Technol 160:1–8. https://doi.org/10.1016/j.jmatprotec.2004.01.001
8. Na YS, Yeom JT, Park NK, Lee JY (2003) Simulation of microstructures for Alloy 718 blade forging using 3D FEM simulator. J Mater Process Technol 141:337–342. https://doi.org/10.1016/S0924-0136(03)00285-1

9. Chen F, Ren F, Chen J et al (2016) Microstructural modeling and numerical simulation of multi-physical fields for martensitic stainless steel during hot forging process of turbine blade. Int J Adv Manuf Technol 82:85–98. https://doi.org/10.1007/s00170-015-7368-8
10. Lin YC, Chen MS, Zhong J (2008) Numerical simulation for stress/strain distribution and microstructural evolution in 42CrMo steel during hot upsetting process. Comput Mater Sci 43:1117–1122. https://doi.org/10.1016/j.commatsci.2008.03.010
11. Pasoodeh B, Alimirzaloo V, Tagimalek H (2021) The numerical and experimental evaluation of upsetting process of hexagonal cylindrical billet of AISI-1045 steel. The 6th International and 17th National Conference on Manufacturing Engineering Tehran, Iran
12. Wen DX, Wang JK, Wang K et al (2019) Hot tensile deformation and fracture behaviors of a typical ultrahigh strength steel. Vacuum 169:108863. https://doi.org/10.1016/j.vacuum.2019.108863
13. Zhang Y, Guo B, Li Q et al (2021) Damage and cracking prediction of AISI 410 martensitic stainless steel at elevated temperatures. Steel Res Int 92:1–12. https://doi.org/10.1002/srin.202100030
14. Cockcroft MG, Latham DJ (1968) Ductility and the Workability of Metals. J Inst Met 96, pp 33–39
15. Oyane M, Sato T, Okimoto K, Shima S (1980) Criteria for ductile fracture and their applications. J Mech Working Technol 4. https://doi.org/10.1016/0378-3804(80)90006-6
16. Brozzo P, Deluca B, Rendina R (1972 Oct 9) A new method for the prediction of formability limits in metal sheets. In: Proc 7th biennal Conf IDDR
17. Clift SE, Hartley P, Sturgess CEN, Rowe GW (1990) Fracture prediction in plastic deformation processes. Int J Mech Sci 32:1–17. https://doi.org/10.1016/0020-7403(90)90148-C
18. Freudenthal FA (1950) The inelastic behaviour of solids. Wiley, New York, pp 1–70
19. Dourandish S, Champliaud H, Morin J-B, Jahazi M (2022) Microstructure-based finite element modeling of a martensitic stainless steel during hot forging. Int J Adv Manuf Technol. https://doi.org/10.1007/s00170-022-10306-z
20. Hensel A, Spittel T (1978) Kraft- und Arbeitsbedarf bildsamer Formgebungsverfahren, 1. Auflage. VEB Deutscher Verlag für Grundstoffindustrie, Leipzig SE
21. Sellars CM, McTegart WJ (1966) On the mechanism of hot deformation. Acta Metall 14(9):1136–1138
22. Jin Z, Li K, Wu X, Dong H (2015) Modelling of microstructure evolution during thermoplastic deformation of steel by a finite element method. Mater Today: Proc 2:S460–S465. https://doi.org/10.1016/j.matpr.2015.05.062
23. Hallberg H (2011) Approaches to modeling of recrystallization. Metals 1:16–48. https://doi.org/10.3390/met1010016
24. Sellars CM, Whiteman JA (1979) Recrystallization and grain growth in hot rolling. Metal Sci 13. https://doi.org/10.1179/msc.1979.13.3-4.187
25. Jonas JJ, Poliak EI (2003) The critical strain for dynamic recrystallization in rolling mills. Mater Sci Forum 426–432:57–66. https://doi.org/10.4028/www.scientific.net/msf.426-432.57
26. Ghazani MS, Eghbali B (2018) A ductile damage criterion for AISI 321 austenitic stainless steel at different temperatures and strain rates. Arab J Sci Eng 43:4855–4861. https://doi.org/10.1007/s13369-018-3191-5
27. Dhondapure P, Tize Mha P, Nayak S et al (2023) Influence of deformation path on the stress state and damage evolution along the central axis of a large size forged ingot of AISI H13 steel. J Mater Res Technol 27:8244–8257. https://doi.org/10.1016/j.jmrt.2023.11.206
28. Momeni A, Ebrahimi GR, Jahazi M, Ezatpour HR (2024) Microstructure characterization and dynamic recrystallization behavior of Ni–Cu alloy during hot deformation. Mech Mater 193:105002. https://doi.org/10.1016/j.mechmat.2024.105002